9A.3 CROSS-COUPLING, ANTENNA ERRORS AND SIMULTANEOUS HORIZONTAL AND VERTICAL POLARIZATION TRANSMIT DATA

J.C. Hubbert*, S.M. Ellis, G. Meymaris and M. Dixon
National Center for Atmospheric Research, Boulder CO

1. INTRODUCTION

The simultaneous transmission and reception of H (horizontal) and V (vertical) polarized waves (called SHV mode) has become a very popular way to achieve dual polarization for weather radar (Doviak et al. 2000). The advantage is that a fast polarization switch is not necessary to achieve dual polarization data. The disadvantages are 1) that the linear depolarization ratio (LDR) is not measured and 2) that there can be cross-coupling of the H and V waves which will lead to measurement biases, especially differential reflectivity (Z_{dr}). The viability of this dual polarization technique is base on 1) non-zero mean canting angle of the propagation medium, and 2) negligible antenna polarization errors. If either condition is not met, cross-coupling between the H and V channels occurs which will cause measurement biases.

Measurement errors in the SHV mode have been investigated. Doviak et al. (2000) evaluated cross-coupling errors of SHV mode and concluded that since the mean canting angle of rain is zero, the errors were acceptable. Wang and Chandrasekar (2006) investigated the measurement errors in Z_H (reflectivity), Z_{dr}, ϕ_{dp} and ρ_{hv} due to cross-coupling errors caused by the radar system. They concluded that system isolation between the the H and V channels must be greater than -44 dB in order to insure the Z_{dr} bias is within 0.2 dB for worst case errors.

Ryzhkov and Zrnić (2007) examined the effects of non-zero mean canting angle of the precipitation medium on SHV mode measurements. Data gathered in SHV mode with KOUN (NSSL's S-band research radar) displayed Z_{dr} radial bias "stripes" after the radar waves passed through the ice phase of either convective cells or stratiform precipitation. They propose that non-zero mean canting angle of the propagation medium causes coupling between the H and V polarized waves that causes the anomalous Z_{dr} signatures.

All reflector type antennas will introduce some distortion to the desired H and V transmit polarization states causing cross coupling between the H and V polarization states. This will bias polarization measurements of precipitation. These errors are similar to the cross-coupling problem reported in Ryzhkov and Zrnić (2007). This paper investigates the impact of antenna induce cross-coupling errors caused by the non ideal radar antenna. The radar model introduced by Hubbert and Bringi (2003) is used to quantify the impact of polarization errors on Z_{dr} and ϕ_{dp}. Finally experimental data from S-Pol, NCAR's S-band polarimetric radar, are used to illustrate the theory. Recently, S-Pol collected data in fast alternating H and V transmit mode (referred to as FHV mode) quickly followed by data collected in simultaneous H and V transmit mode (referred to as SHV mode). These data clearly illustrate the effects of antenna polarization errors. This is the first time that such data has been collected and analyzed.

*NCAR/EOL, Boulder, Colorado 80307, email: hubbert@ucar.edu

2. MODELING POLARIZATION ERRORS AND CROSS-COUPLING

The scattering model used is described in Hubbert and Bringi (2003) but is briefly reviewed here. The particles in the backscatter volume and the coherent propagation medium are independently modeled. The "steady" propagation medium is modeled via a 2×2 matrix that includes absolute attenuation (A_h), differential attenuation (A_{dp}), differential propagation phase (ϕ_{dp}) and mean canting angle (θ) as parameters. The resolution volume (or backscatter medium) is modeled as an ensemble of precipitation particles with Gamma DSD (drop size distribution) and arbitrary spatial orientation distributions via the T-matrix method (Vivekanandan et al., 1991; Waterman, 1969). The modeled parameters can be independently varied so that the sensitivity of the crosspolar and co-to-cross covariances can be studied. Antenna polarization errors are modeled similar to McCormick (1981) and Bringi and Chandrasekar (2001).

In this paper, the antenna polarization errors and cross coupling caused by non-zero mean canting angle are the focus and the backscatter medium is not considered. The mean canting angle, α, of the precipitation particles in the backscatter medium is set to zero.

2.1. *Antenna Polarization Errors*

The radar antenna and surrounding microwave circuitry introduce microwave cross-coupling that give rise to polarization errors so that pure H or V polarization are not

transmitted. Polarization errors have been covered in detail by McCormick (1981). Some of the sources of polarization error are non-ideal feed horn, non ideal parabolic reflector, antenna support struts and edge effects. These polarization errors are distributed across the radar antenna patterns and thus can vary across the beam especially where the cross-polarized lobes exist (Bringi and Chandrasekar 2001). For distributed precipitation media, the resulting error is an integrated effect and we model these distributed errors with a 2×2 polarization error matrix as is done in Bringi and Chandrasekar (2001)

The polarization errors are easily included in the model by pre- and post- multiplying $\mathbf{S}$, the 2×2 backscatter matrix, by the error matrix Υ

$$\mathbf{S_e} = \mathbf{\Upsilon}^T \mathbf{S} \mathbf{\Upsilon} \tag{1}$$

where

$$\mathbf{\Upsilon} = \begin{bmatrix} i_h & \varepsilon_v \\ \varepsilon_h & i_v \end{bmatrix}. \tag{2}$$

with constraints $i_h^2 + |\varepsilon_h|^2 = i_v^2 + |\varepsilon_v|^2 = 1$ with i_h, i_v real. The polarization errors of the H and V channels are represented by the complex numbers ε_h and ε_v, respectively. The polarization errors can also be equivalently represented with the geometric ellipse parameters of tilt angle, τ and ellipticity angle, ϵ. These variables are related by (Azzam and Bashara, 1989)

$$\tan 2\tau = \frac{2\Re(\chi)}{1-|\chi|^2} \tag{3}$$

$$\sin 2\epsilon = \frac{2\Im(\chi)}{1+|\chi|^2} \tag{4}$$

where χ is the polarization ratio define by $\chi = E_v/E_h$ where E_v and E_h are the vertical and horizontal electric field components, and $\Re$ and $\Im$ denote real and imaginary parts, respectively. For H errors, $\chi = \varepsilon_h/i_h$ and for V errors, $\chi = i_v/\varepsilon_v$. As can be seen from the equations, if the ε_h (ε_v) is real then ϵ is zero and if ε_h (ε_v) is imaginary then τ is zero. If the errors are orthogonal, i.e., $\varepsilon_v = -\varepsilon_h^*$, then Υ is unitary and (1) represents an orthogonal change of polarization basis. Separating the polarization errors into their geometric components gives a convenient and intuitive way to analyze polarization errors.

2.2. *Modeling Simultaneous H and V transmissions*

The model thus far was constructed under the assumption that the radar is operating in FHV (fast alternating H and V) mode. The backscatter covariance matrix is a convenient form for expressing the radar covariances and for polarization bases transformations; however, it does not function as a transmission matrix, i.e., it does not express a transfer relationship between an arbitrary input polarization and the resultant output covariances such as the 4×4 Mueller matrix does (Bringi and Chandrasekar 2001). In order to model output covariances that result from arbitrary transmit polarizations, a 4×4 covariance matrix is formed using the feature vector

$$\mathbf{\Omega}^T = [S_{HH}\ S_{VH}\ S_{HV}\ S_{VV}] \tag{5}$$

Taking the outer product of of the feature vector gives the covariance matrix in the H-V basis as

$$\mathbf{\Sigma}_0 = \begin{bmatrix} \langle|S_{HH}|^2\rangle & \langle S_{HH}S_{VH}^*\rangle & \langle S_{HH}S_{HV}^*\rangle & \langle S_{HH}S_{VV}^*\rangle \\ \langle S_{VH}S_{HH}^*\rangle & \langle|S_{VH}|^2\rangle & \langle S_{VH}S_{HV}^*\rangle & \langle S_{VH}S_{VV}^*\rangle \\ \langle S_{HV}S_{HH}^*\rangle & \langle S_{HV}S_{VH}^*\rangle & \langle|S_{HV}|^2\rangle & \langle S_{HV}S_{VV}^*\rangle \\ \langle S_{VV}S_{HH}^*\rangle & \langle S_{VV}S_{VH}^*\rangle & \langle S_{VV}S_{HV}^*\rangle & \langle|S_{VV}|^2\rangle \end{bmatrix} \tag{6}$$

where $\langle\cdot\rangle$ denotes spatial or temporal averages. Note that the covariance matrix is Hermitian. It an be shown that the matrix of Eq.(6) is easily transformed to the Mueller matrix and thus the covariance matrix of Eq.(6) can also be used as a transfer function matrix:

$$\mathbf{J_o} = \mathbf{\Sigma}_0\, \mathbf{J}_i \tag{7}$$

where $\mathbf{J}_i$ and $\mathbf{J}_o$ are $1\times$ 4 input and output coherency matrices. In terms of the desired polarization characteristics of the incident polarization, namely tilt angle (τ) and ellipticity angle (ϵ), $\mathbf{J}_i$ becomes

$$\mathbf{J}_i = \begin{bmatrix} J_{i1} \\ J_{i2} \\ J_{i3} \\ J_{i4} \end{bmatrix} = \begin{bmatrix} 1+\cos 2\tau \cos 2\epsilon \\ \sin 2\tau \cos 2\epsilon - j \sin 2\epsilon \\ \sin 2\tau \cos 2\epsilon + j \sin 2\epsilon \\ 1-\cos 2\tau \cos 2\epsilon \end{bmatrix} \tag{8}$$

If linear slant 45° incident is desired (i.e. SHV mode), then $\tau = 45°$ and $\epsilon = 0°$. The SHV variables of interest can be calculated as

$$Z_{dr}^{shv} = 10\log_{10}[J_{o1}/J_{o4}] \tag{9}$$

$$\Psi_{dp}^{shv} = \tan^{-1}(\Im\{J_{o3}\}/\Re\{J_{o3}\}) \tag{10}$$

$$\rho_{hv}^{shv} = \frac{|J_{o2}|}{\sqrt{|J_{o1}||J_{o4}|}} \tag{11}$$

where the superscript "shv" denotes SHV mode.

3. MODEL RESULTS

Next we examine biases in Z_{dr}^{shv} caused by 1) transmit errors, and 2) non-zero mean propagation canting angle. Antenna polarization errors. are considered later. Again, the radar variables are plotted as a function of principal plane ϕ_{dp}^{P}. Since ϕ_{dp}^{P} is the independent variable and since K_{dp} i is of more meteorological interest than ϕ_{dp}, normalize SHV K_{dp} is expressed as:

$$K_{dp}^{Nshv} = \frac{K_{dp}^{shv}}{K_{dp}^{P}} \tag{12}$$

where K_{dp}^{Nshv} is normalize SHV K_{dp}, K_{dp}^{shv} is SHV K_{dp} and K_{dp}^{P} is principal plane K_{dp}. Absolute attenuation $A_h = 0.0165$ dB/deg. and differential attenuation $A_{dp} = 0.0035$ dB/deg. which are typical S-band values. The model shows that K_{dp}^{shv} errors are less than 3% for antenna errors that correspond to a LDR system limit of -25 dB. This quite small for this relatively large antenna error and thus K_{dp}^{shv} are not given here.

3.1. *Transmit Errors*

Z_{dr}^{shv} is plotted as a function of ϕ_{dp}^{P}. The transmit polarization state is specified with the complex transmit H and V electric fields, E_h^t and E_v^t. This is not the electric field that emerges from the the antenna but is rather the electric field that in injected into the wave guides that feed the antenna. For SHV mode, ideally $E_h^t = E_v^t$. Figure 1 shows Z_{dr} when $|E_h^t| \neq |E_v^t|$, the mean canting angle of the precipitation medium is zero degrees and the antenna polarization are zero, i.e., $\varepsilon_h = \varepsilon_v = 0$. The Z_{dr} bias is independent of the phase difference between E_h^t and E_v^t. The slope of the curves is caused by $A_{dp} = 0.0035$dB/deg. The red nominal line is considered ideal. As can be seen the biases are constant as compared to the nominal curve and such biases could be corrected via calibration.

3.2. *Non-zero Mean Canting Angle*

The model is now used to illustrate Z_{dr} bias caused by non-zero mean canting angle of the propagation medium. Antenna errors are zero and the transmit errors are zero, i.e., $E_h^t = E_v^t$. Figure 2 shows just the Z_{dr} bias as a function of ϕ_{dp}^{P} with the mean canting angle of the propagation medium as a parameter. As the mean canting angle increases, the bias increases. If the principal plane $\phi_{dp} < 10^\circ$, the biases are kept to within about 0.1 dB. Figure 3 is similar to Fig. 2 except that the phase difference between E_h^t and E_v^t is 90°, i.e., the transmit polarization is circular. The Z_{dr} bias (the difference between the SHV mode Z_{dr} and the nominal line) now increases much more rapidly as a function of ϕ_{dp}^{P} as compared to Fig. 2. Now ϕ_{dp}^{P} needs to be less than about 1 degree in order to kept Z_{dr} bias less than about 0.1 dB. This then shows that if the mean canting angle of ice particles is not zero, very little differential phase needs to accumulate in order to cause significant Z_{dr} bias. This corroborates the findings of Ryzhkov and Zrnić (2007).

4. ESTIMATING ANTENNA POLARIZATION ERRORS

The estimation of the complex error terms, ε_h and ε_v, is difficult and they are typically not supplied by the manufacturer. There are ways, however, to estimate the magnitude of the error terms and to generally qualify their character. Two available quantities are, LDR (Linear Depolarization Ratio) and passive sun calibration measurements.

LDR can be expressed as a function of the polarization errors ε_h and ε_v (Bringi and Chandrasekar 2001). The radar system lower limit of LDR can be estimated by measurements in drizzle where raindrops are considered circular so that the intrinsic LDR is $-\inf$ dB. Measured LDR is then an estimate of the radar system isolation between the H and V channels. For well designed radars, the dominant cross coupling factor is the antenna. The received voltages can be modeled in drizzle as

$$\begin{bmatrix} V_h^r \\ V_v^r \end{bmatrix} = \begin{bmatrix} i_h & \varepsilon_h \\ \varepsilon_h & i_v \end{bmatrix} \begin{bmatrix} 1 & 0 \\ 0 & 1 \end{bmatrix} \begin{bmatrix} i_h & \varepsilon_v \\ \varepsilon_h & i_v \end{bmatrix} \begin{bmatrix} E_h^t \\ E_v^t \end{bmatrix} \tag{13}$$

where the identity matrix is the backscatter matrix for drizzle. For transmit state $E_h^t = 1$, $E_v^t = 0$, LDR is

$$LDR_\ell = \frac{|\langle \varepsilon_v i_h + \varepsilon_h i_v \rangle|^2}{|\langle i_h^2 + \varepsilon_h^2 \rangle|^2} \tag{14}$$

Using the approximations $|\varepsilon_{h,v}| \ll i_{h,v}$ and $i_h = i_v \approx 1$, it follows that

$$LDR_\ell = |\varepsilon_h + \varepsilon_v|^2 = |\varepsilon_h|^2 + |\varepsilon_v|^2 + 2\Re\{\varepsilon_v \varepsilon_h^*\} \tag{15}$$

where LDR_ℓ is linear LDR and $\Re$ stands for the the real part.

The LDR system limit values are typically in the -30 to -34 dB range for well designed radars. If $\varepsilon_h = \varepsilon_v$ and ε_h and ε_v are real (or imaginary) then $LDR = 10\log_{10}(2\varepsilon_h)^2 = -30$ dB, and therefore $\varepsilon_h = \varepsilon_v = 0.0158$. If the LDR limit is -35 dB, then $\varepsilon_h = \varepsilon_v = 0.00889$. Equivalently, these errors correspond to a tilt and ellipticity angles of the polarization state (polarization ellipse) of the received wave. The angles are 0.91∘ and 0.51° for LDR limits of -30 dB and -35 dB, respectively. If the ε_h and ε_v are real, the angles are tilt angles, and if the ε_h and ε_v are imaginary, the angles are ellipticity angles.

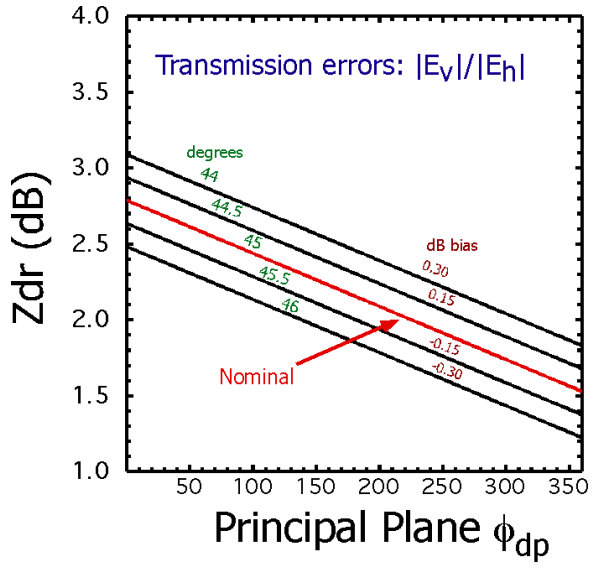

Figure 1: *Z_{dr} as a function of principal plane ϕ_{dp} with unbalanced transmit power as a parameter. For SHV mode, $|E_h^t| = |E_v^t|$ and this curve is shown as nominal in red. The errors are independent of the phase difference between E_h^t and E_v^t.*

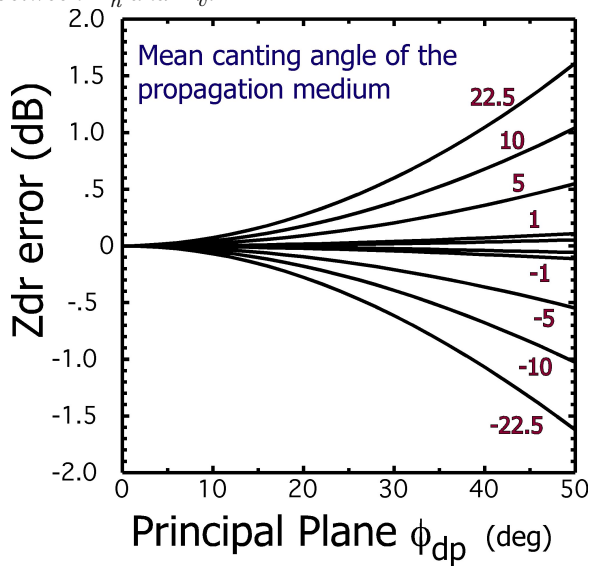

Figure 2: *Z_{dr} bias as a function of principal plane ϕ_{dp} with the mean canting angle of the propagation medium as a parameter. There transmission errors are zero, i.e., $|E_h^t| = |E_v^t|$. The errors are independent of the phase difference between E_h^t and E_v^t.*

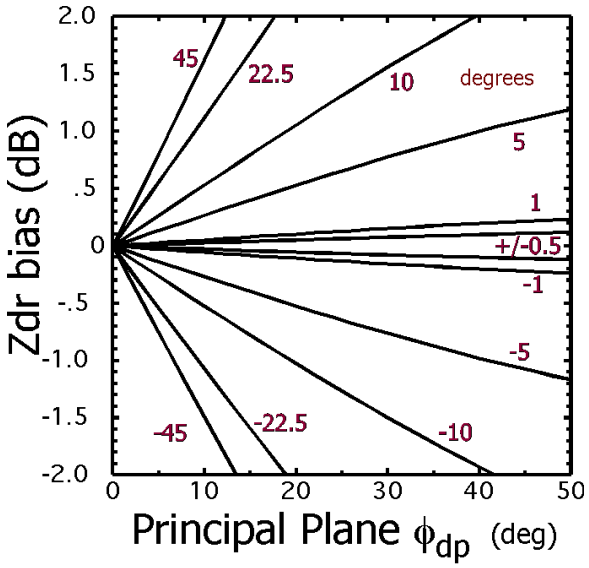

Figure 3: *Z_{dr} bias as a function of principal plane ϕ_{dp} with the mean canting angle of the propagation medium as a parameter. $|E_h^t| = |E_v^t|$ but there is a 90° phase difference, i.e., circular polarization is transmitted.*

4.1. *Solar Scan Measurements*

The solar data is collected performing a "box scan" of the sun in passive mode. The sun here is considered as an unpolarized RF source that has a width of about 0.53° (Tapping 2001). The dimensions of the box scan are approximately 3° high (elevation angle) by 7° wide (in azimuth). Noise samples are collected while the radar is pointing away from the the sun so that the thermal background noise can be estimated and used to correct the measured sun data. The typical scanning rate is $1°s^{-1}$. The data is interpolated to a square 2° by 2° in 0.1° intervals. The data is first corrected for sun movement and distortion caused by scanning in elevation and azimuth angle rather than in a rectangular grid. Shown in Fig. 4 are the H and V pseudo antenna patterns obtained from such solar scans. These are termed pseudo antenna patterns since the sun is not a point source and thus the given antenna patterns are a convolution of the antenna beam pattern of S-Pol with the 0.53° solar disk. The complex H and V antenna data can be used to create a correlation antenna pattern. The receive voltage time series, $V_h^r(i)$ and $V_v^r(i)$ for the H and V patterns, respectively, are correlated in typical fashion as

$$\omega = \frac{\sum_{i=1}^{N} V_h(i) V_v^*(i)}{\sqrt{\sum_{i=1}^{N} V_h(i) V_h^*(i) \sum_{i=1}^{N} V_v(i) V_v^*(i)}} \qquad (16)$$

Equation (16) represents the correlation between the H and V received voltages for a single point in azimuth and

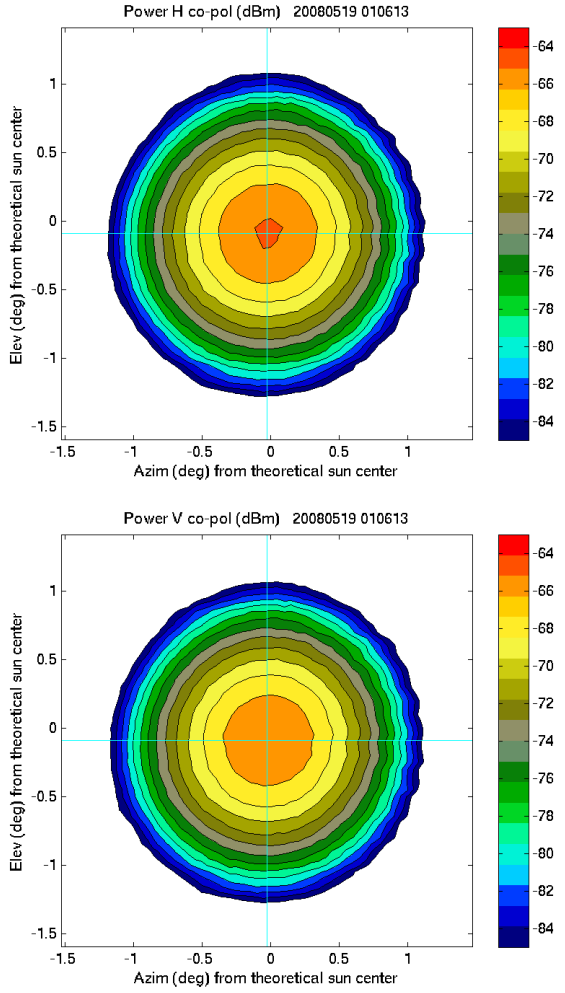

Figure 4: *Pseudo H (top) and V (bottom) S-Pol antenna patterns obtained by scanning the sun passively.*

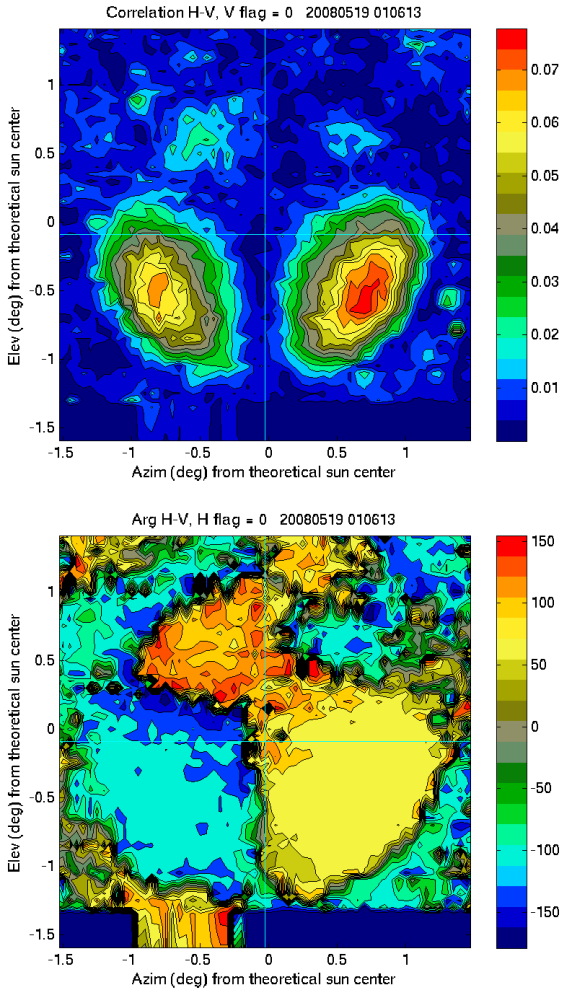

Figure 5: *Pseudo H to V correlation S-Pol antenna patterns obtained by scanning the sun passively. Top panel in the magnitude and the bottom panel is differential phase.*

elevation angle. This data can also be interpolated to a grid. The resulting magnitude (top) and phase (bottom) of the correlation product of Eq. (16) are give in Fig. 5. Since the sun radiation is unpolarized, the correlation between any two orthogonal polarization state should be zero. The top panel of the figure shows two principal "lobes" in the lower two quadrants where the correlation increases to about 0.07. These large areas of increased correlation coefficient are manifestation of the antenna polarization errors. The cross-correlation is obviously a function of azimuth and elevation angle and is not constant across the 2° by 2° antenna patterns shown. The areas of maximum correlation do, however, fall outside the 3 dB beamwidth of the antenna which is about 1°. The bottom panel of Fig. 5 shows the complex behavior

of the phase of the correlation products with the phases being fairly constant in the regions of highest correlation. For the lower left quadrant this phase is -100° while the lower right quadrant phase is about 60°.

The radar model presented above represents the antenna polarization errors as a single complex number numbers for the H and V polarization, i.e., the polarization errors are considered constant across the entire radar antenna pattern. This representation of polarization errors assumes that the scattering medium is homogeneous across the entire radar antenna pattern. It is usually sufficient (for well designed antennas) if the scattering medium is homogeneous across the first two or three degrees of the antenna pattern centered on copolar patterns maximum (bore sight).

It can be shown that for small antenna polarization errors that

$$\Omega = \varepsilon_h^* + \varepsilon_v \tag{17}$$

where Ω is the antenna pattern integrated correlation coefficient and ε_h and ε_v are the antenna polarization errors as given in Eq.(2). Thus, the correlation products are averaged across the entire given 2° by 2° correlation beam pattern of Fig. 5 to arrive at a single complex number. This would be valid if the radar is scanning a uniform, homogeneous region.

Solving Eqs.(15) and (17) simultaneously yields

$$\Im\{\varepsilon_v\} = \frac{\Im\{\Omega\} \pm \sqrt{\Im^2\{\Omega\} - 4(|\Omega|^2 - LDR_\ell)}}{2} \tag{18}$$

$$\Im\{\varepsilon_h\} = \frac{-\Im\{\Omega\} \mp \sqrt{\Im^2\{\Omega\} - 4(|\Omega|^2 - LDR_\ell)}}{2} \tag{19}$$

In term of the voltages, the solutions are

$$\Im\{\varepsilon_h\} = \frac{\Im\{ldr\} - \Im\{\Omega\}}{2} \tag{20}$$

$$\Im\{\varepsilon_v\} = \frac{\Im\{ldr\} + \Im\{\Omega\}}{2} \tag{21}$$

The real parts are not solvable but it can be shown they obey the condition

$$\Re\{ldr\} - \Re\{\Omega\} = 0 \tag{22}$$

where ldr is the complex number $\varepsilon_h + \varepsilon_v$ (see Eq.(15)).

4.2. *Antenna Errors*

Figure 6 show SHV mode Z_{dr} for one degree polarization tilt errors (upper panel) and one degree polarization ellipticity errors (lower panel). Such errors correspond to an LDR system limit of about -30 dB. The solid straight lines represent non-biased Z_{dr} that would be measured in fast alternating transmit mode. As can be seen, Z_{dr} errors are significant with a maximum error of about 0.6 dB.

	H tilt	H ellip.	V tilt	V ellip.
A	-0.5°	-0.7°	89.5°	0.7°
B	0.5°	-0.7°	90.5°	0.7°
C	-0.5°	0.7°	89.5°	-0.7°
D	0.5°	0.7°	90.5°	-0.7°

Table 1: *The H and V tilt and ellipticity error angles corresponding to 7.*

	LDR (dB)	$\Im\{\xi_h\} \approx \epsilon$ (rad.)	ϵ (deg.)
A	-25	0.0281	1.61°
B	-30	0.016	0.91°
C	-35	0.009	0.509°
D	-40	0.005	0.286°
E	-45	0.003	0.161°

Table 2: *Antenna polarization errors as a function of system LDR limit. The antenna errors are assumed to be orthogonal and elliptical.*

Figure 7 shows Z_{dr} bias for mixed tilt and ellipticity angles. The H and V tilt and ellipticity angles are given in Table 1. As can be seen, the character of the Z_{dr} bias is quite different for each curve with the maximum bias is about 0.4 dB for each curve. This antenna errors all correspond to about a -31 dB system LDR limit. These same antenna errors from Table 1 are used again in Fig. 8, but for circular transmit polarization. The Z_{dr} biases curves have changed dramatically and demonstrate the importance of the phase difference between the H and V components of the transmit wave.

4.3. *Analysis and Interpretation*

Casting the antenna errors in terms of tilt and ellipticity angles of thge polarization ellipse provides insight as to to the nature of the errors. From knowledge of the LDR system limit (about -31 dB) and solar data we can write

$$\sqrt{LDR_\ell} = |\xi_h + \xi_v| = 0.0282 \tag{23}$$

$$|\Omega| = |\xi_h^* + \xi_v| = 0.0039 \tag{24}$$

where 0.0039 was obtained from S-Pol solar scans measurements. Since the real parts of Eqs. (23) and (24) are equal, the only way for $|\Omega| \ll \sqrt{LDR_\ell}$ is for the $\Im\{\xi_h\} \approx \Im\{\xi_v\}$. In terms of the ellipticity angles, $\epsilon_h \approx -\epsilon_v$. *This means that the antenna ellipticity error angles are nearly orthogonal.* We assume that the feed horn is designed well and aligned so that the tilt error angle is very small. Additionally, the H and V tilt angle errors must also be nearly orthogonal since non-orthogonal

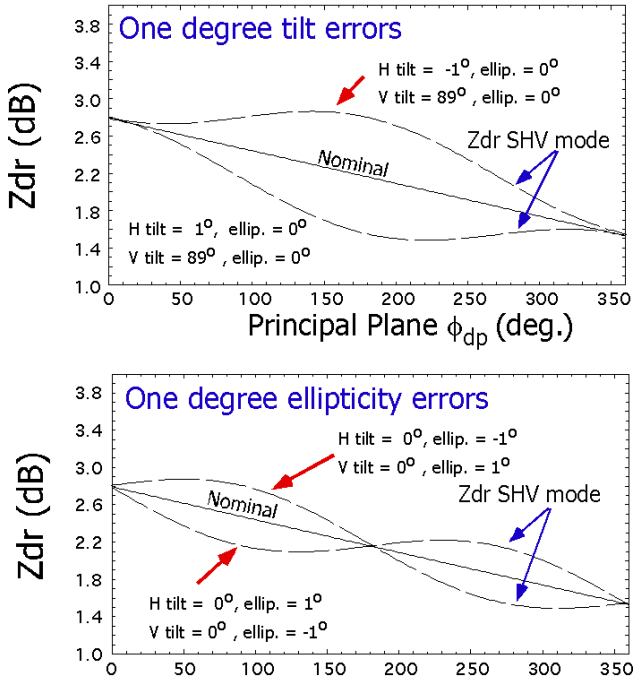

Figure 6: *SHV mode Z_{dr} for one degree antenna polarization errors. The upper panel shows $\pm 1^{\circ}$ tilt errors while the lower panel shows $\pm 1^{\circ}$ ellipticity errors.*

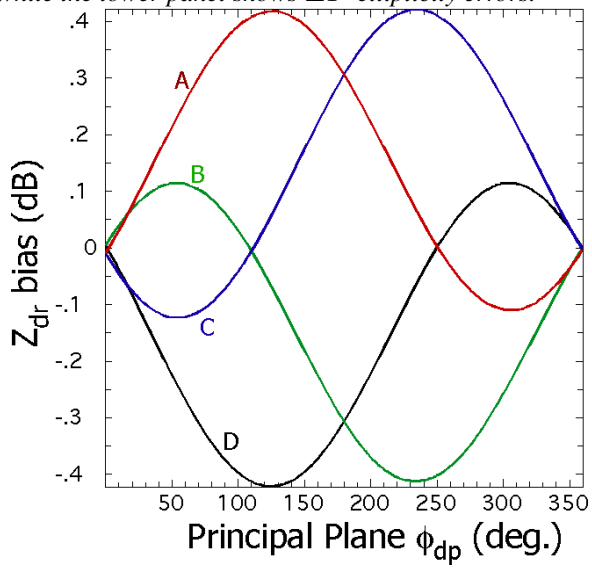

Figure 7: *SHV mode Z_{dr} for mixed tilt and ellipticity antenna error angles which are given in Table 1. These antenna error correspond to a system LDR limit is -30 dB.*

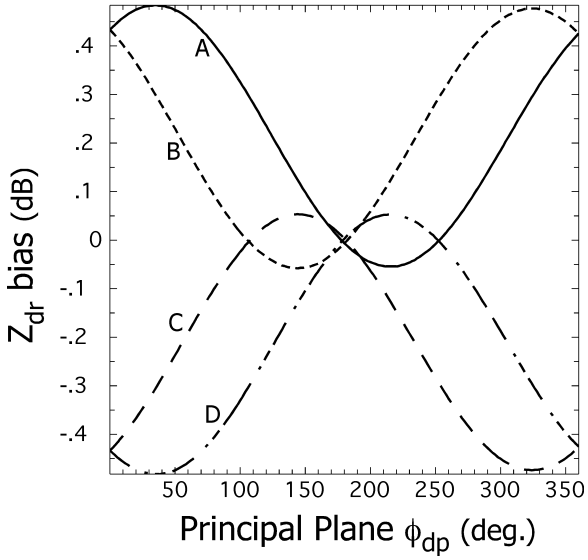

Figure 8: *SHV mode Z_{dr} for mixed tilt and ellipticity antenna error angles which are given in Table 1, however, the transmission polarization state is circular. The antenna errors are orthogonal. These antenna errors correspond to a system LDR limit of -31 dB.*

tilt errors will cause both ξ_h and ξ_v to increase. Thus, the antenna polarization errors for S-Pol are well characterized by orthogonal ellipticity antenna errors. Under these conditions, the H and V ellipticity angles are found to be, $\epsilon_h = -0.91^{\circ}$ and $\epsilon_v = 0.69^{\circ}$.

The LDR system limit for a radar can be related to the SHV Z_{dr} bias as a function of ϕ_{dp}^{P} with differential transmit phase as a parameter. Based on the antenna errors for S-Pol, the antenna errors are model as orthogonal ellipticity angles with no tilt angle errors. This is shown in Fig. 9 for (a) slant 45° linear transmit polarization (i.e., $E_h^t = E_v^t$) and (b) circular transmit polarization. The shown ϵ denotes the sign of the H polarization ellipticity angle. The values of the ellipticity angle corresponding to each curve are given in Table 2. Note how not only the shape of bias curves changes but also the maximum Z_{dr} bias increases significantly for circular transmit polarization. The model shows that the most stringent crosspolar isolation criteria results from the circular polarization transmit condition. As can be seen, if SHV Z_{dr} bias is to be kept under 0.2 dB, the LDR system limit needs to be about -40 dB. Practically, if one of circular transmit bias curves characterized a radar, the Z_{dr} bias at $\phi_{dp} = 0$ would likely be detected by the user and a Z_{dr} offset correction factor would be used. Then, the maximum Z_{dr} bias would occur for $\phi_{dp}^{P} = 180^{\circ}$.

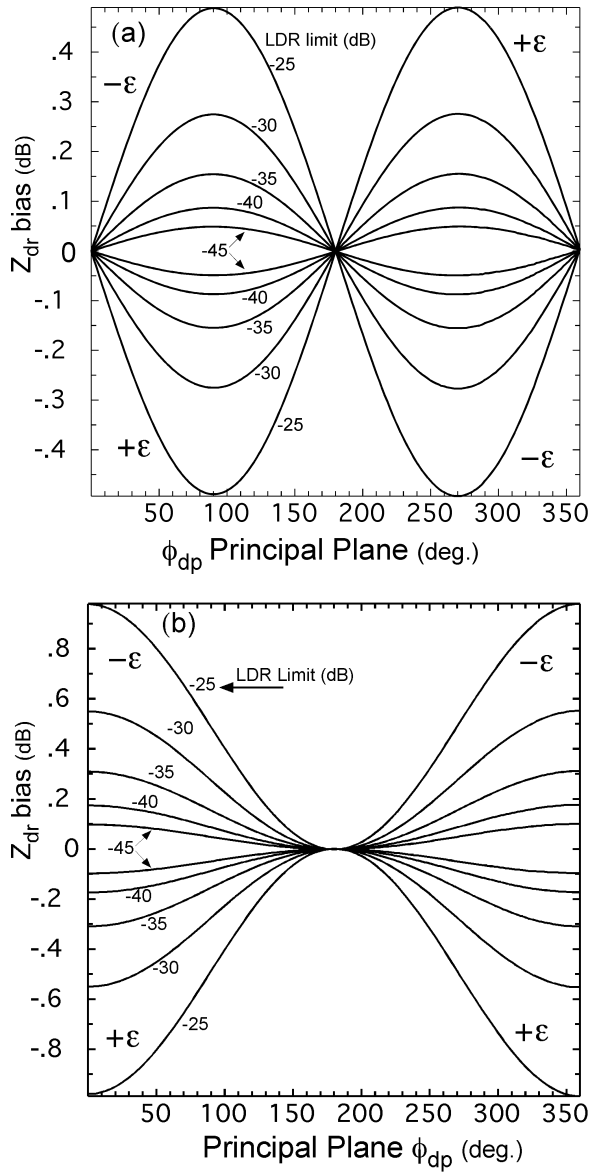

Figure 9: *SHV mode Z_{dr} bias as a function of principal plane ϕ_{dp} with LDR system limit as a parameter. The antenna polarization errors are assumed to be orthogonal ellipticity angles. The sign of the H ellipticity angle is given in each quadrant. (a) The transmit polarization is 45° linear, i.e., $E_h^t = E_v^t$. The curves all mimic a sine wave shape. (b) The transmit polarization is circular. The curves are symmetric about the vertical line through 180°. The corresponding antenna errors are given in Table 2.*

5. EXPERIMENTAL SHV DATA

During May and June 2008, S-Pol was deployed in Southern Taiwan for the field experiment TiMREX (Terrain-influenced Monsoon Rainfall Experiment) where data were collected in the SHV mode. Normally S-Pol operates in the FHV mode. Thus, SHV and FHV data that were gathered only minutes apart can be compared. Two cases are examined: 1) 8.6° elevation data and 2) 2.0° elevation data. The first case demonstrates Zdr bias due to non-zero mean canting angle in the ice phase and the second data set demonstrates Z_{dr} bias due to antenna polarization errors in rain

5.1. *SHV Z_{dr} Bias in Ice*

Figures 10 and 11 show S-Pol FHV mode reflectivity (Z) and differential reflectivity (Z_{dr}) gathered during TiMREX on 2 June 2008, 6:19:36 UTC at 8.6° elev. Figures 12 and 13 show SHV Z and Z_{dr} gathered at 6:13:59 UTC at 8.6° elev. A line of convective cells is on the eastern edge with trailing stratiform rain to the west. Storm cells were moving west to east. At about 35 km range, high and noisy Z_{dr} marks the brightband. Note the azimuthal "striping" of Z_{dr} in the SHV mode Z_{dr} data beyond the brightband in Fig. 13. No Z_{dr} striping is evident in the FHV Z_{dr} data of Fig. 10. The Z_{dr} striping in Fig. 13 is likely due to non-zero mean canting angle of the ice particles in the propagation path in agreement with Ryzhkov and Zrnić (2007).

5.2. *SHV Z_{dr} Bias in Rain*

Figures 14 and 15 show S-Pol FHV mode reflectivity (Z) and differential reflectivity (Z_{dr}) gathered during TiMREX on 2 June 2008, 6:17:06 UTC at 2.0° elev. Figures 16 and 17 show SHV Z and Z_{dr} gathered at 6:11:28 UTC at 2.0° elev. There is no Z_{dr} striping evident in the SHV data of Fig. 17 since the elevation angle is low and most of the data is in rain which has zero mean canting angle. The SHV and FHV Z_{dr} data appear fairly comparable but in fact there is a bias in the SHV data. To show this, we employ the self consistency Z calibration technique of Vivekanandan et al. (2003). The technique is based on the relationship of Z, Z_{dr} and ϕ_{dp} in rain. Based on the typical range of rain drop size and shape distributions, ϕ_{dp} can be estimated based on measured Z and Z_{dr}. This estimated ϕ_{dp} (ϕ_{dp}^e) is compared to the measured ϕ_{dp} (ϕ_{dp}^m). A scatter plot is generated and a straight line fit is calculated. If the calculated mean line differs from the 1-to-1 line, this indicates a reflectivity bias. The technique assumes that Z_{dr} is well calibrated (S-Pol Z_{dr} is calibrated via vertical pointing data in light rain).

Shown in Fig.18 is a scatter plot of ϕ_{dp}^e versus ϕ_{dp}^m for

TiMREX data. The Z bias is about 0.03 dBZ, i.e., negligible. Note the tight scatter about the 1-to-1 line. This indicates that S-Pol is well calibrated and such self consistency plots are the norm for S-Pol. Fig. 19 is similar to Fig. 18 except the data was gathered in SHV mode. The scatter is rather tight about the 1-to-1 line for $\phi_{dp} < 50^\circ$ but for $\phi_{dp} > 70^\circ$ the computed ϕ_{dp} are biased low. This is due antenna errors.

To further illustrate this SHV Z_{dr} bias, Z_{dr} is averaged under the constraint 20 dBZ$< Z \leq 25$ dBZ. These Z_{dr} data are partitioned into three categories: 1) $20^\circ < \phi_{dp} < 40^\circ$, 2) $40^\circ < \phi_{dp} < 70^\circ$, and 3) $70^\circ < \phi_{dp} < 100^\circ$. The results are given in Table 3. For low ϕ_{dp} the SHV and FHV Z_{dr} values are about equal. For $40^\circ < \phi_{dp} < 70^\circ$, the Z_{dr}s differ by 0.11 dB and for $70^\circ < \phi_{dp} < 100^\circ$ the Z_{dr}s differ by 0.27 dB. The data is not corrected for differential attenuation (which could add potential error). This increasing difference between FHV and SHV Z_{dr} as a function of ϕ_{dp} is consistent with the Z_{dr} bias predicted for antenna errors of radar systems with LDR limit in the -30 dB to -35 dB range.

5.3. *Quantifying and Correcting Z_{dr} Bias Caused by Antenna Polarization Errors*

To support the assertion that the FHV and SHV Z_{dr} differences seen above are a result of antenna polarization errors, the S-Pol antenna errors calculated above are now used in the model to compute an estimated SHV Z_{dr} bias. The errors are $\tau_h = 0^\circ$, $\epsilon_h = -0.91^\circ$ and $\tau_v = 90^\circ$, $\epsilon_v = 0.69^\circ$ which corresponds to $\xi_h = -j0.0159$ and $\xi_v = -j0.0120$. This is not to say that these are the precise S-Pol antenna errors but they do characterize the antenna errors well as is demonstrated next. These estimated antenna errors are used in the model and the results are shown in Fig. 20. There are no transmit errors and the mean canting angle of the propagation medium is zero. As is seen, the Z_{dr} bias becomes more positive with increasing ϕ_{dp} in a similar fashion to that in the above experimental data. The model also predicts that in FHV mode, the measured LDR_h (LDR for H polarization transmission) *decreases* with increasing ϕ_{dp} instead of increasing due to differential attenuation as normally expected. This type of LDR_h behavior is observed with S-Pol data for long paths of increasing ϕ_{dp}. Thus, the model predicts well the general behavior of the observed SHV Z_{dr} bias and FHV LDR_h.

Finally, the SHV experimental data of Fig. 19 are corrected using the the modeled Z_{dr} bias values from Fig. 20 as a function of measured ϕ_{dp}. The self consistency technique is then again applied to the corrected data and the result is shown in Fig. 21. As can be seen the data are now better clustered around the one-to-one line as compared to the uncorrected data of Fig. 19.

6. CONCLUSIONS

Simultaneous transmission of H and V polarization waves (termed SHV mode) is now a popular way to construct dual-polarization radar systems. The technique is based on the assumption of 1) zero-mean canting angle of the precipitation medium and 2) negligible antenna polarization errors. Zero-mean canting angle is a good approximation for rain but not for the ice phase of storms. SHV data from S-Pol during TiMREX showed Z_{dr} biases in the ice phase of storms are are likely due to a non-zero mean canting angle of the the ice particles. This corroborates well with Ryzhkov nd Zrnić (2007) similar findings.

Antenna errors were modeled and the SHV Z_{dr} biases were examined. Experimental data were used to estimated the LDR system limit (about -31 dB) and the H to V solar scan correlation coefficient. Using these measurements, It was shown that the antenna errors of S-Pol were well characterized by orthogonal ellipticity errors. Additionally, the S-Pol antenna error ellipticity angles were estimated.

SHV and FHV data from the field experiment TiMREX were used to demonstrate the SHV Z_{dr} biases. The SHV Z_{dr} bias in rain was shown to be a function of ϕ_{dp} with a maximum bias of about 0.3 dB at 100 degrees of ϕ_{dp} accumulation. The antenna errors as estimated from the LDR system limit and solar H and V correlation values were used in the model to predict the SHV Z_{dr} bias. The modeled SHV Z_{dr} bias agreed very well with the demonstrated experimental SHV Z_{dr} bias.

The model showed that if SHV Z_{dr} bias is to be kept to within 0.2 dB, the system limit LDR should be less that -40 dB. This is a very difficult performance figure to achieve for center-fed parabolic reflector antennas. a low LDR limit gure may not be cost-effective to achieve with center-feed parabolic antennas and this cost must be considered against the afore-mentioned cost-benets of implementing SHV mode dual-polarization.

Acknowledgment

This research was supported in part by the ROC (Radar Operations Center) of Norman OK. The National Center for Atmospheric Research is sponsored by the National Science Foundation. Any opinions, findings and conclusions or recommendations expressed in this publication are those of the author(s) and do not necessarily reflect the views of the National Science Foundation.

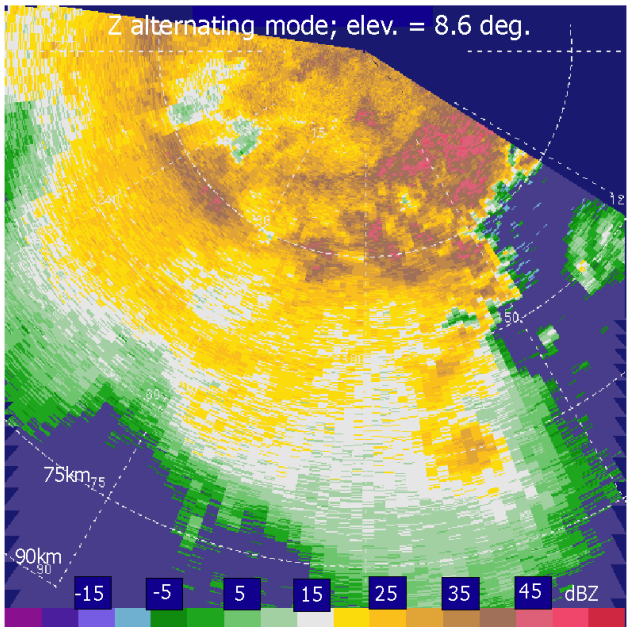

Figure 10: *FHV mode reflectivity for 8.6° elev.*

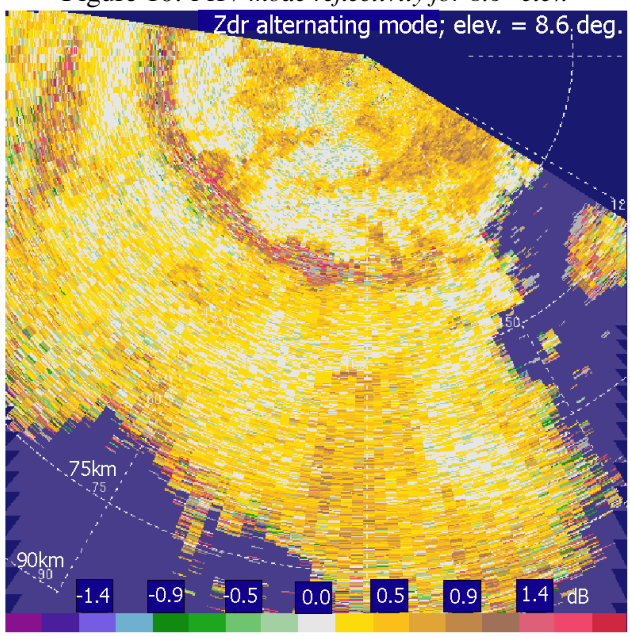

Figure 11: *FHV mode Z_{dr} for 8.6° elev. corresponding to Fig. 10.*

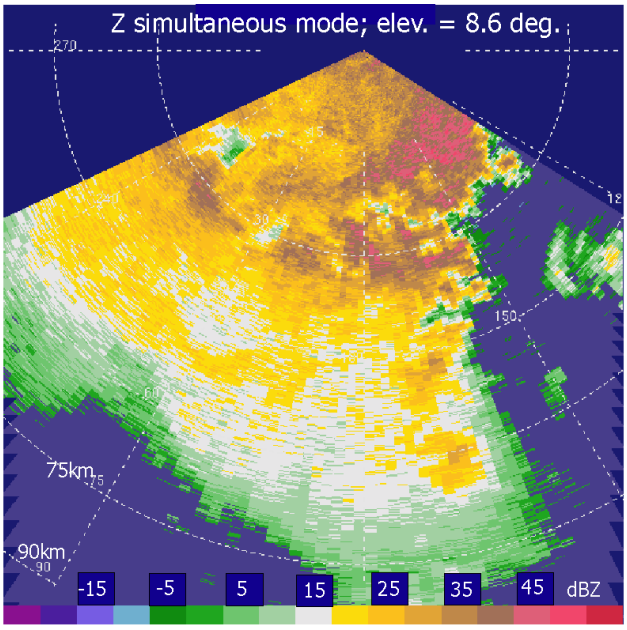

Figure 12: *SHV mode reflectivity for 8.6° elev.*

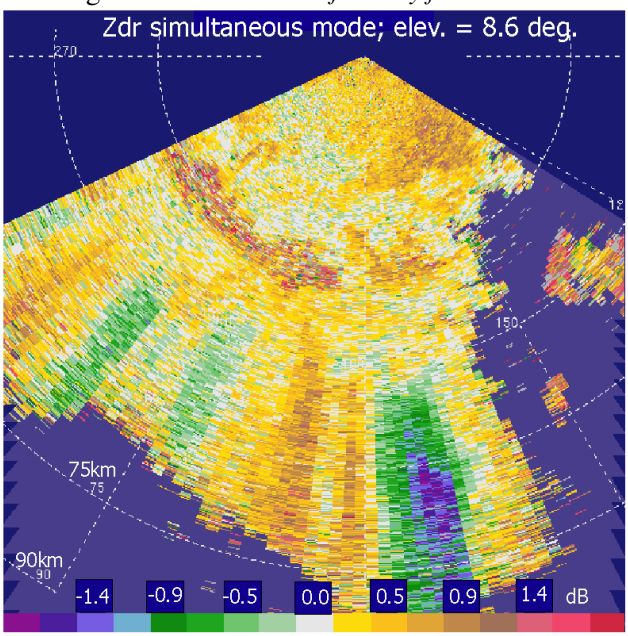

Figure 13: *SHV mode Z_{dr} for 8.6° elev. corresponding to Fig. 12.*

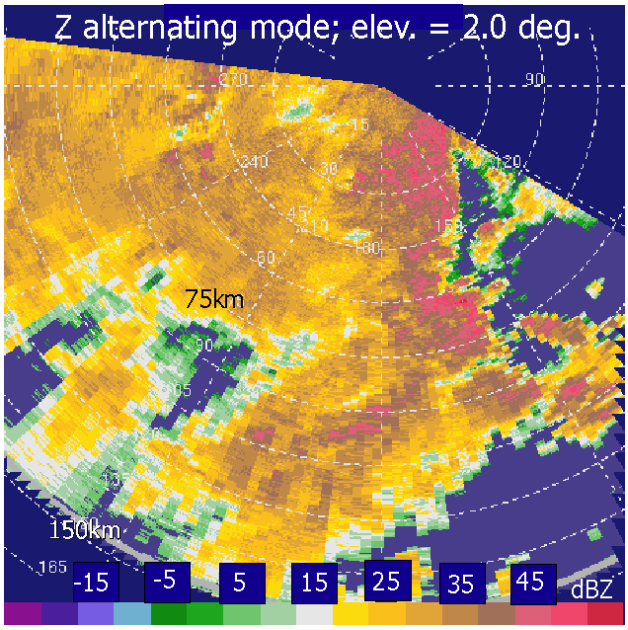

Figure 14: *FHV mode reflectivity for 2.0° elev.*

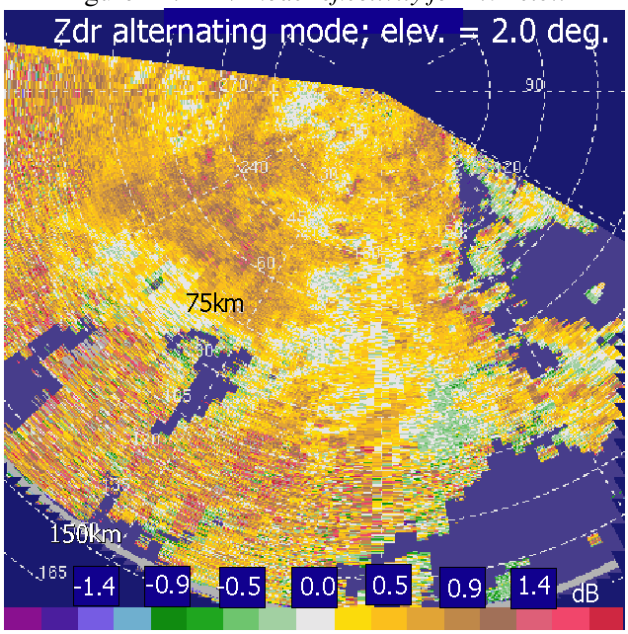

Figure 15: *FHV mode Z_{dr} for 2.0° elev. corresponding to Fig. 14.*

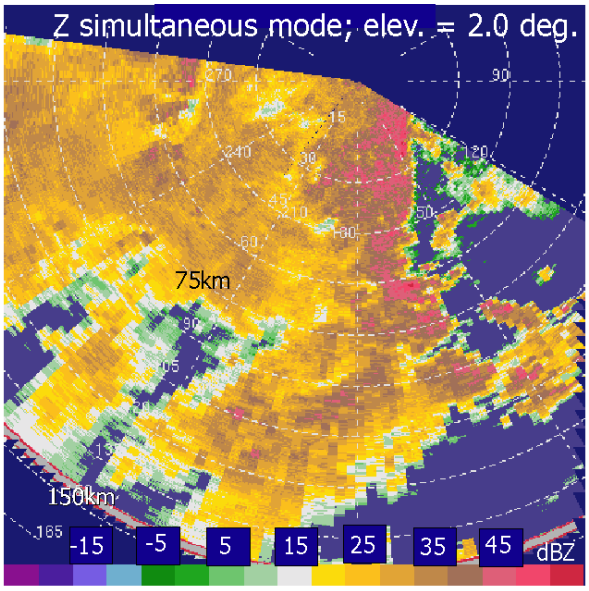

Figure 16: *SHV mode reflectivity for 2.0° elev.*

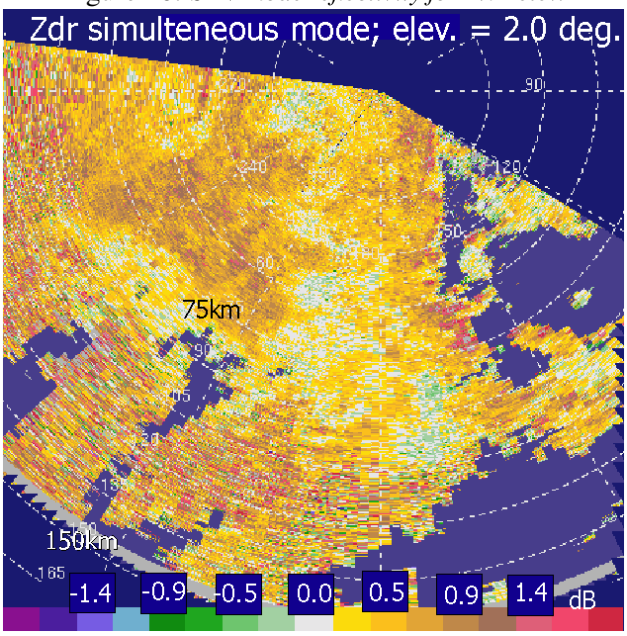

Figure 17: *SHV mode Z_{dr} for 2.0° elev. corresponding to Fig. 16.*

Total ϕ_{dp}	Mean Z_{dr} (dB)	
	FHV	SHV
between 20 and 40 deg.	0.17	0.16
between 40 and 70 deg.	0.15	0.26
between 70 and 100 deg.	-0.07	0.20

Table 3: *A comparison of Z_{dr} values for FHV and SHV modes as a function of ϕ_{dp}. Reflectivities are limited to between 20 and 25 dBZ.*

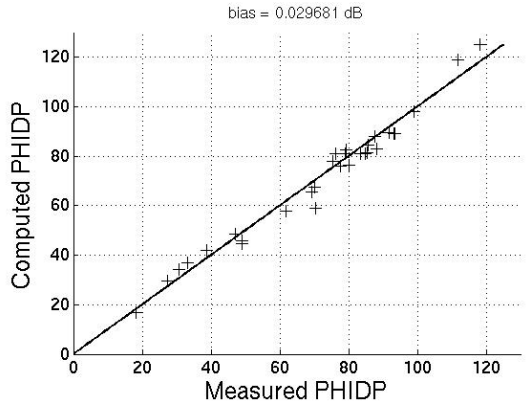

Figure 18: *Scatter plot of calculated ϕ_{dp} (from Z and Z_{dr}) versus measured ϕ_{dp} from TiMREX FHV data. The Z bias is about 0.03 dBZ.*

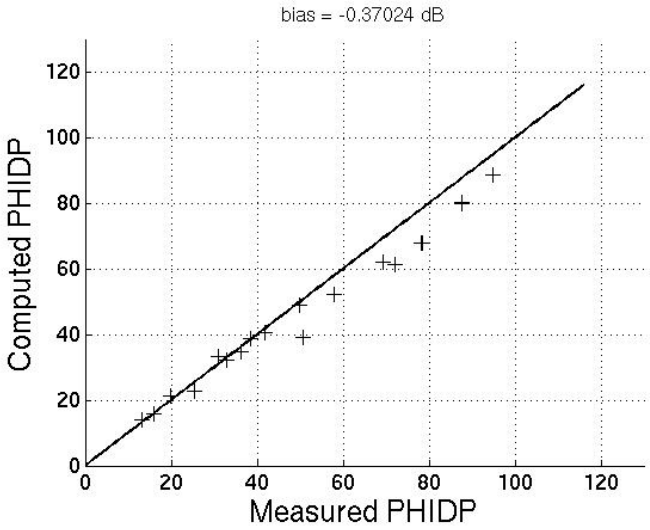

Figure 19: *Scatter plot of calculated ϕ_{dp} (from measured Z and Z_{dr}) versus measured ϕ_{dp} from TiMREX SHV data. The Z bias is about -0.37 dBZ but this is not the cause of the bias of the points for high ϕ_{dp}. It is bias of Z_{dr} for high ϕ_{dp} which is the cause.*

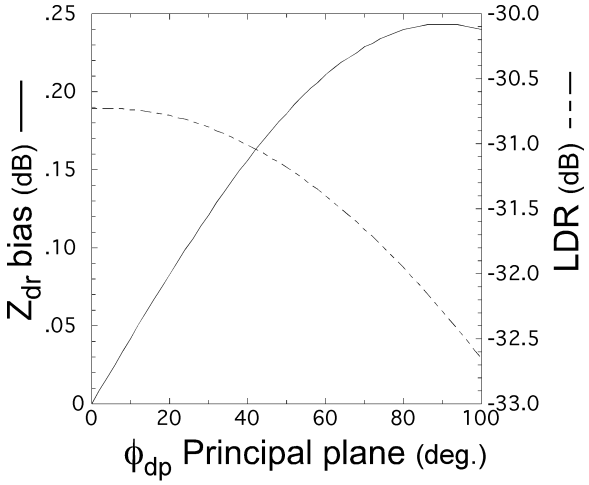

Figure 20: *SHV mode Z_{dr} and FHV mode LDR_h from the model. The antenna polarization errors are $\tau_h = 0°$, $\epsilon_h = -0.91°$ and $\tau_v = 90°$, $\epsilon_v = 0.69°$.*

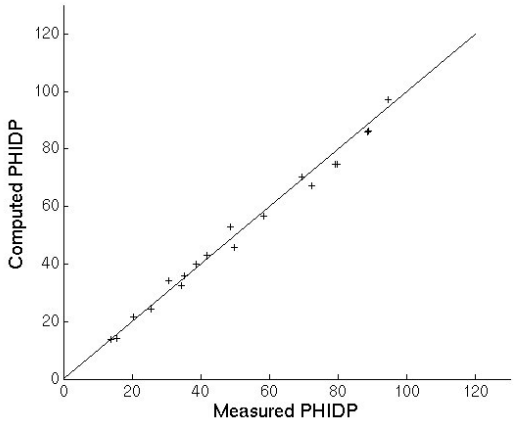

Figure 21: *Scatter plot of calculated ϕ_{dp} (from measured Z and Z_{dr}) versus measured ϕ_{dp} from TiMREX SHV data from Fig. 19 except the Z_{dr} is corrected as a function of measured ϕ_{dp} using the relationship in Fig. 20.*

References

Azzam, R. and N. Bashara, 1989: *Ellipsometry and polarized light*. North Holland, Amsterdam.

Bringi, V. and V. Chandrasekar, 2001: *Polarimetric Doppler Weather Radar*. Cambridge Univ. Press, Cambridge, UK.

Doviak, R., V. Bringi, A. Ryzhkov, A. Zahrai, and D. Zrnić, 2000: Polarimetric upgrades to operational WSR-88D radars. *J. Atmos. Oceanic Technol.*, **17**, 257–278.

Hubbert, J. and V. Bringi, 2003: Studies of the polarimetric covariance matrix: Part II: Modeling and polarization errors. *J. Atmos. Oceanic Technol.*, 1011–1022.

McCormick, G., 1981: Polarization errors in a two-channel system. *Radio Sci.*, **16**, 67–75.

Ryzhkov, A. and D. Zrnić, 2007: Depolarization in ice crystals and its effect on radar polarimetric measurements. *J. Atmos. Oceanic Tech.*, **24**, 1256–1267.

Tapping, K.: 2001, Antenna calibration using the 10.7 cm solar flux. *Radar Polarimetry for geoscience applications*, P. Smith, ed., American Meteorological Society, http://cdserver.ametsoc.org/cd/010430_1/RADCAL_Links_2_Presentations.html.

Tragl, K., 1990: Polarimetric radar backscattering from reciprocal random targets. *IEEE Trans. Geosc. and Remote Sen.*, **8**, 856–864.

van de Hulst, H., 1957: *Light scattering by small particles*. New York: Wiley.

Vivekanandan, J., W. Adams, and V. Bringi, 1991: Rigorous approach to polarimetric radar modeling of hydrometeor orientation distributions. *J. Appl. Meteorol.*, **30**, 1053–1063.

Vivekanandan, J., G. Zhang, S. Ellis, D. Rajopadhyaya, and S. Avery, 2003: Radar reflectivity calibration using differential propagation phase measurement. *Radio Sci.*, **38**, 8049.

Wang, Y. and V. Chandrasekar, 2006: Polarization isolation requirements for linear dual-polarization weather radar in simultaneous transmission mode of operation. *IEEE Trans. Geosc. and Remote Sen.*, **44**, 2019–2028.

Waterman, P., 1969: Scattering by dielectric particles. *Alta Frequeza,(Speciale)*, 348–352.